

Superconducting and Antiferromagnetic Properties of Dual-Phase V_3Ga

Michelle E. Jamer,¹ Brandon Wilfong,¹ Vasily D. Buchelnikov,^{2,3} Vladimir V. Sokolovskiy,^{2,3} Olga N. Miroshkina,^{2,4} Mikhail A. Zagrebina,^{2,5} Danil R. Baigutlin,^{2,4} Jared Naphy,¹ Badih A. Assaf,⁶ Laura H. Lewis,⁷ Aki Pulkkinen,⁴ Bernardo Barbiellini,^{4,8} Arun Bansil,⁸ and Don Heiman⁸

¹Physics Department, United States Naval Academy, Annapolis, MD 20899, USA

²Faculty of Physics, Chelyabinsk State University, 454001 Chelyabinsk, Russia

³National University of Science and Technology "MISIS", 119049 Moscow, Russia

⁴Department of Physics, School of Engineering Science, LUT University, FI-53851 Lappeenranta, Finland

⁵National Research South Ural State University, 454080 Chelyabinsk, Russia

⁶Physics Department, University of Notre Dame, South Bend, IN 46556

⁷Chemical Engineering Department, Northeastern University, Boston, MA

⁸Physics Department, Northeastern University, Boston, MA

(Dated: 1 June 2020)

The binary compound V_3Ga can exhibit two near-equilibrium phases, consisting of the A15 structure that is superconducting, and the Heusler $D0_3$ structure that is semiconducting and antiferromagnetic. Density functional theory calculations show that the two phases are closely degenerate, being separated by only ± 10 meV/atom. Magnetization measurements on bulk-grown samples show superconducting behavior below 14 K. These results indicate the possibility of using V_3Ga for quantum technology devices utilizing both superconductivity and antiferromagnetism at the same temperature.

I. Introduction

Combining superconductivity and antiferromagnetism could find useful applications in quantum spintronic devices. Superconductivity and magnetism were once thought to be mutually exclusive, as magnetic fields are efficient at closing the superconducting gap. Nevertheless, it was found that superconducting materials could contain $3d$ magnetic transition metal atoms and magnetic lattices as well¹. Following that, high- T_c cuprate superconductors were found to have exceedingly strong magnetic exchange², while superconducting Fe-pnictides were found to have large Fe moments of several Bohr magnetons^{3,4}. Of interest here are binary vanadium compounds such as V_3Al that belong to a class of simple superconductor materials with A15 crystal structure⁵⁻⁸. Interestingly, V_3Al was also synthesized in a non-superconducting $D0_3$ Heusler phase with antiferromagnetic (AFM) order⁹. This $D0_3$ phase of V_3Al was predicted to be a gapless semiconductor^{10,11}, and was found experimentally⁹ to be a G-type antiferromag-

net having a Neél temperature of $T_N = 600$ K. One can draw the conclusion that V_3Z -type compounds represent a class of hybrid materials with superconducting and magnetic properties at the same temperature, which could have applications in possible fault-tolerant quantum computers hosting Majorana modes and in other important quantum technology applications.

Another well-known compound in this family is V_3Ga , which has been used in superconducting applications for many years¹². This material has been known since 1956 to have remarkable low-temperature properties related to elastic constants, Knight shifts, electrical resistance, magnetic susceptibility, superconductivity and it has been investigated extensively both experimentally and theoretically (see e.g. Refs.¹³⁻¹⁹). The critical temperature of superconducting V_3Ga in the A15 phase is 14 K.

V_3Ga can exist in two near-equilibrium phases, the A15 superconducting phase and the AFM $D0_3$ phase - an interesting and potentially useful result of their similar formation energies. Since the arrangement of atoms in binary V_3Ga can accommodate both $D0_3$ and A15 structures, shown in Fig. 1, one must study the stability of these two phases. Density functional theory (DFT) was used here to compute the formation energies as a function of crystalline and magnetic structures. Previous theoretical calculations for the $D0_3$ structure of V_3Ga by Galanakis *et al.*¹¹ have predicted a Heusler G-type AFM phase with a Neél temperature well above room temperature, which makes the compound attractive for applications^{9,20,21}. A recent study also reported on the similar formation energies of the two structures.²² The present magnetization measurements on bulk samples show a strong Meissner effect indicating a superconducting transition temperature of 14 K.

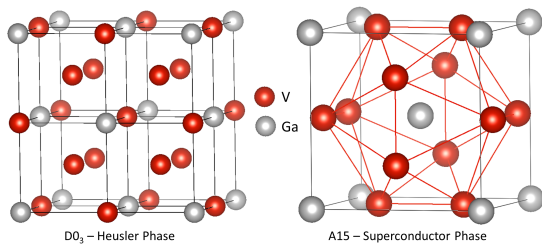


FIG. 1. $D0_3$ (space group $Fm\bar{3}m$ no. 225, prototype BiF_3) and β -W A15 (space group $Pm\bar{3}n$ no. 223, prototype Cr_3Si) crystal structures of V_3Ga .

II. Experimental Details and Results

Bulk samples of V_3Ga were synthesized via arc-melting using an Edmund Buehler MAM-1. The ingots were subsequently annealed at $1050^\circ C$ for 48 hours in an Argon environment to promote homogeneity and quenched in an ice bath. The composition was confirmed using energy dispersive spectroscopy (EDS) to be within $\pm 2\%$ of the nominal composition. Magnetic measurements were performed in a Quantum Design MPMS XL-5 SQUID magnetometer in magnetic fields up to 5 T and temperatures from $T = 2$ to 400 K. Synchrotron X-ray diffraction was done using beamline 11-BM at the Advanced Photon Source (APS). The structure was refined using TOPAS.²³ Overall, the structural results determined that there was a mixed phase of both A15 and $D0_3$ of V_3Ga . The Rietveld refinement analysis determined that the A15 was the predominant phase at 81% and the $D0_3$ accounted for 19% of the structural analysis (Supplemental Information).

Results of the magnetic measurements are shown in Figs. 2 and 3. In particular, Fig. 2 shows a magnetic hysteresis from the Meissner effect at low temperature, which is characteristic of flux pinning of the A15 type-II superconducting phase. The superconducting transition temperature $T_c = 13.6$ K is deduced from the plot of the magnetization as a function of temperature as shown in the inset of Fig. 2. Dimensionless magnetic susceptibility is shown in Supplemental Information which indicates $\sim 90\%$ superconducting volume fraction in line with expectations from the compositional analysis of the X-ray diffraction data through Rietveld refinement. The inset of Fig. 3 shows the magnetic moment as a function of applied field at $T = 300$ K. The moment is linear up to at least $\mu_0 H = 5$ T, where the moment is only $\mu = 0.007 \mu_B$ per formula unit (f.u.). This linear-in-H moment is similar to that found in the AFM $D0_3$ phase of V_3Al ⁹. A focus on the superconducting properties of the A15 phase is presented in Supplemental Information which shows an H_{c2} of about 3.5 T for isothermal magnetization at 10 K. This value is significantly lower than the previously accepted value of 15 T at 10 K for the A15 V_3Ga phase.^{24,25} The decrease in H_{c2} is most likely due to the antiferromagnetic phase from the $D0_3$ component which attributes significant magnetic signal at higher field. Previous reports of off-stoichiometry A15 V_3Ga ²⁴ did not alter the H_{c2} as drastically as the observed in the current system, therefore it is reasonable to attribute this significant decrease in H_{c2} as due to the antiferromagnetic signal of another magnetic V_3Ga phase present in the as-synthesized compound mixture. At higher temperatures there is a notable peak in the temperature dependence of the low-field ($H = 500$ Oe) moment at $T = 360$ K, shown in Fig. 3. A similar feature was seen in the temperature-dependent resistivity of V_3Ga at 350 K²², however, the peak was not assigned to a magnetic transition. The similar temperature-dependent features in both the magnetization and the resistivity could arise from either a

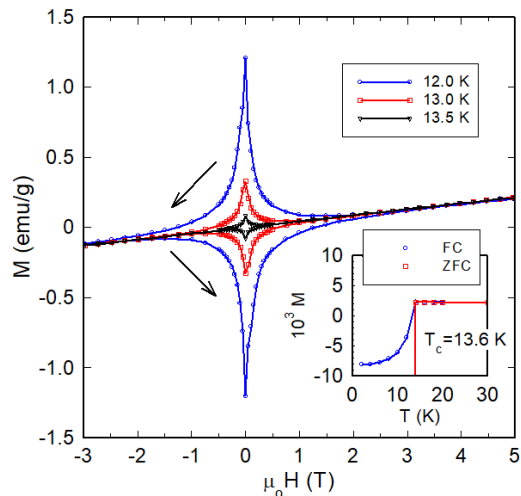


FIG. 2. Magnetization of superconducting V_3Ga versus magnetic field at low temperatures under Zero field cooling (ZFC), showing a hysteretic peak around $H = 0$ characteristic of flux pinning in a type-II superconductor. The inset shows the temperature-dependent Meissner flux exclusion below $T_c = 13.6$ K taken in a field of $H = 500$ Oe.

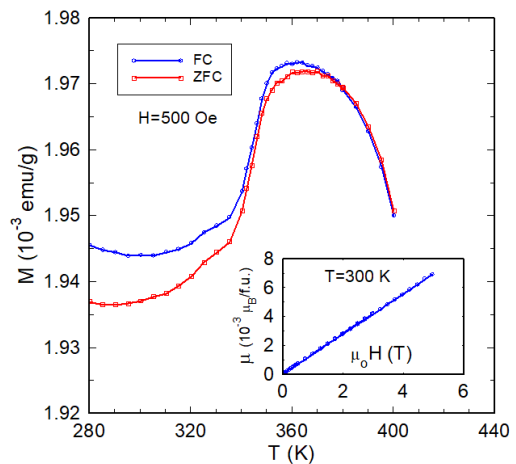


FIG. 3. Magnetic properties of AFM V_3Ga versus temperature and magnetic field. Magnetization versus temperature taken at $H = 500$ Oe shows a peak at 360 K, indicating a magnetic transition. (inset) Magnetic moment versus magnetic field taken at $T = 300$ K, showing a small moment of only $\mu = 0.007 \mu_B/f.u.$ at $\mu_0 H = 5$ T.

structural or a magnetic transition. A small peak in the magnetization of an AFM is generally characteristic of a Neel temperature⁹, so there is a reasonable case to assign the small peak observed here in the magnetization of V_3Ga to some type of magnetic transition.

TABLE I. The calculated equilibrium magnetic states (*Mag. st.*), lattice constants (a_0 in Å), atom-resolved and total magnetic moments (μ_{V_i} and μ_{tot} in μ_B /f.u.), total energy (E_0 in eV/atom), as well as the energy difference between the D0₃ and A15 structures (ΔE_{D0_3-A15} in eV/atom) for V₃Ga. The results are shown for various exchange-correlation approaches described in the text. For the A15 structure, the SCAN solutions for FM and AFM-III are almost degenerate and within 5 meV/atom.

	D0 ₃							A15							ΔE
	<i>Mag. st.</i>	a_0	μ_{V_1}	μ_{V_2}	μ_{V_3}	μ_{tot}	E_0	<i>Mag. st.</i>	a_0	μ_{V_1}	μ_{V_2}	μ_{V_3}	μ_{tot}	E_0	
LDA	AFM	5.902	0.429	-0.429	0.0	0.0	-8.487	FM	4.678	0.089	0.164	0.112	0.368	-8.572	0.085
GGA	AFM	6.064	-1.314	1.314	0.0	0.0	-7.600	FM	4.788	0.222	0.390	0.303	0.916	-7.645	0.045
GGA+ <i>U</i>	AFM	6.130	-1.916	1.917	0.0	0.0	-6.647	AFM-III	4.879	± 1.351	± 1.508	± 1.502	0.0	-6.632	-0.015
SCAN	AFM	6.035	-1.848	1.848	0.0	0.0	-17.486	FM	4.744	0.308	0.523	0.414	1.245	-17.442	-0.044
								AFM-III	4.744	± 0.268	± 0.326	± 0.330	0.0	-17.437	-

III. Computational Details and Results

Density Functional Theory (DFT) within the projector augmented wave (PAW) as implemented in VASP^{26,27} was used for the electronic structure calculations. Various approximations were considered for the exchange-correlation (XC) energy, such as the local density approximation (LDA)²⁸, the generalized gradient approximation (GGA)²⁹⁻³¹, GGA+*U* (with the Hubbard *U* correction), and the strongly constrained and appropriately normed (SCAN) meta-GGA³²⁻³⁴. We have allowed full lattice and spin relaxation. The calculations were converged to an accuracy of 10^{-8} eV, while a convergence criterion in the optimization for the residual forces was 10^{-7} eV/Å. Concerning the GGA+*U*, the Coulomb integrals $U = 2.0$ eV and $J = 0.67$ eV have been used that were provided by He *et al.*²².

The main results are summarized in Table I, while more details are contained in the Supplemental Materials. The general trend of correlation effects beyond GGA is to stabilize the D0₃ solution with respect to the A15 one. The ground state (GS) in both LDA and GGA is the ferromagnetic (FM) phase with A15 structure. When correlation effects are included, the GS becomes the AFM G-type D0₃ solution. Regarding the A15 solution, the effect of correlations is to stabilize an AFM-III solution^{22,35} with respect to FM one. Within SCAN, the FM and AFM-III solutions in the A15 structure are almost degenerate and within 5 meV/atom (FM is marginally more stable). However, GGA+*U* fully stabilizes the AFM-III solution. The AFM-III solution having a net zero magnetic moment is more compatible with the superconducting properties of A15 structure.

Given the observation of the dual phase in the present V₃Ga samples, SCAN may exaggerate the stabilization of the D0₃ solution, while GGA+*U* gives almost degenerate A15 and D0₃ solutions within 15 meV/atom, a value found previously in DFT solutions²² and is in better accord with the experiment. SCAN is also known to exaggerate the magnetic moment of transition metal atoms, which are well described within GGA³⁶⁻³⁸. In order to alleviate this problem, a modification of SCAN with de-orbitalization has been suggested recently³⁹.

The calculated electronic structure is represented by

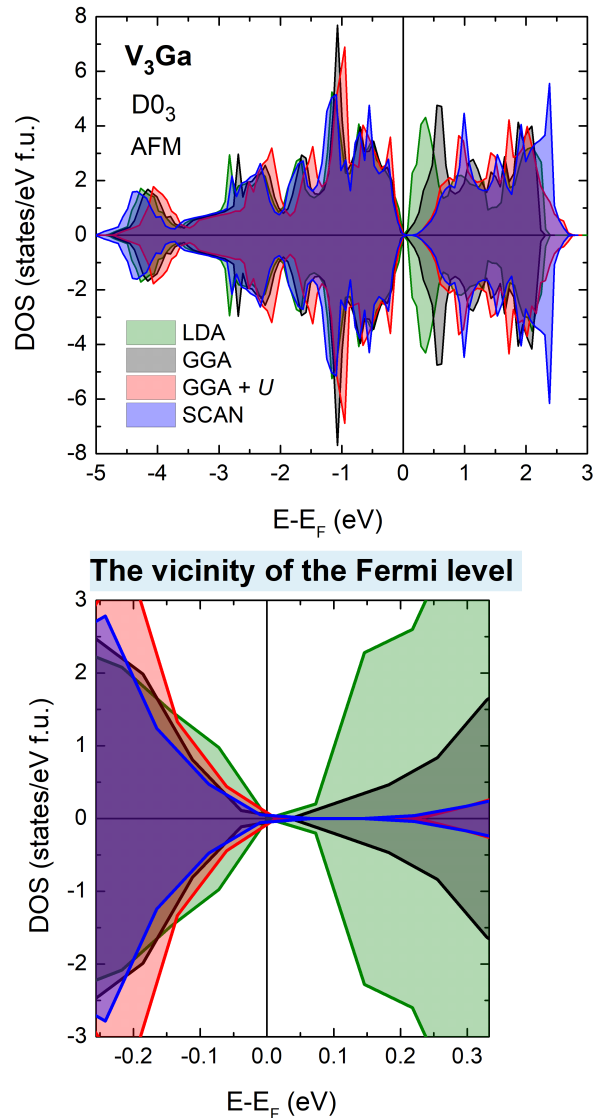


FIG. 4. Total DOS for AFM D0₃ structure calculated with LDA, GGA, GGA+*U* and SCAN methods. The lower figure shows the gapless region near the Fermi level on an expanded energy scale.

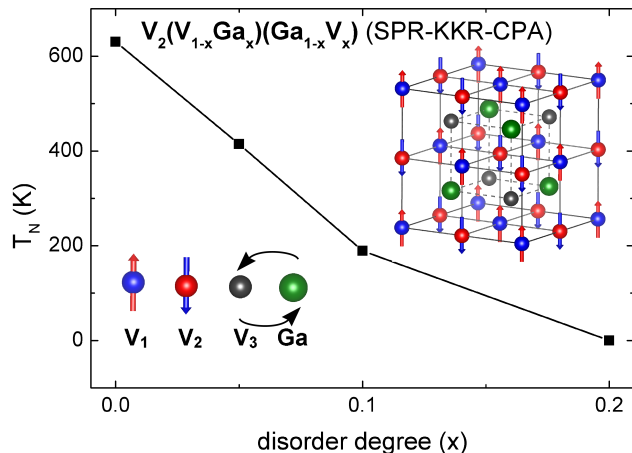


FIG. 5. Dependence of Néel temperature of V_3Ga from disorder using calculations based on SPR-KKR package. Disorder was obtained by exchanging a fraction x of the Ga atoms with the nonmagnetic V atoms. Note that T_N at $x = 0$ here is somewhat larger than that found using a more accurate simulation described in the text.

density of states (DOS) shown in Fig. 4. LDA and GGA schemes give an almost gapless semiconductor, while the effects of correlation beyond GGA within GGA+ U and SCAN lead to the opening of gap with size of about 0.2 eV. Similar gap opening has been observed by Buchelnikov *et al.*⁴⁰ in other Heusler alloys.

In order to estimate the magnetic transition temperature for the AFM G-type $D0_3$ phase, the GGA solution is more appropriate. Using Monte Carlo simulations with *ab initio* exchange integrals and Heisenberg model³⁵, we obtain the Néel temperature $T_N = 590$ K, which is somewhat higher than the peak in the experimental $M(T)$ data at 360 K that was extracted from Fig. 3. However, the Néel temperature is found to be strongly affected by disorder. Effects of disorder on the Néel temperature are calculated by using the mean field approximation implemented in the SPR-KKR packages. Figure 5 illustrates how T_N collapses for increasing disorder when the Ga atoms are exchanged with the nonmagnetic V atoms (those V atoms lying between the two antiferromagnetically coupled magnetic V atoms). It is seen that T_N goes to zero with 20% exchange. Thus, a reduction of the Néel temperature to $T_N = 360$ K would require only 6% of the Ga atoms exchanging for nonmagnetic V atoms. However, we note that there is a sizeable energy barrier for V-Ga exchange. Nevertheless, these results illustrate the importance of the nonmagnetic V atoms to the exchange between the other two antiferromagnetically coupled V atoms.

IV. Conclusions

We have studied the dual-phase superconducting A15 phase and the semiconducting AFM phase $D0_3$ in V_3Ga . To rationalize our results, we have considered several models within DFT. We find that the effect of more accurate XC corrections within DFT is to eliminate or to weaken the total FM moment given by simpler LDA and GGA schemes in the A15 cell. This FM moment could jeopardize the A15 superconducting properties. Correlation effects also tend to stabilize the $D0_3$ solution. However, this trend could be exaggerated within SCAN. Concerning the formation energies, we believe that the most accurate results are between GGA and SCAN, therefore, we deduce that A15 and $D0_3$ phases are degenerate within an uncertainty of about 10 meV/atom. Finally, assuming that GGA gives the best description for the AFM magnetic moments of V atoms in the $D0_3$ solution, we estimated the Néel temperature to be $T_N = 590$ K, but becomes lower with disorder in the atomic sublattices. Finally, the present results indicate the possibility of using V_3Ga for quantum technology devices that require both superconductivity and antiferromagnetism at the same temperature.

Acknowledgments

Use of the Advanced Photon Source at Argonne National Laboratory was supported by the U. S. Department of Energy, Office of Science, Office of Basic Energy Sciences, under Contract No. DE-AC02-06CH11357. The work at Northeastern University was supported by the US Department of Energy (DOE), Office of Science, Basic Energy Sciences Grant No. de-sc0019275 (materials discovery for QIS applications) and benefited from Northeastern University's Advanced Scientific Computation Center and the National Energy Research Scientific Computing Center through DOE Grant No. DE-AC02-05CH11231. The work of Chelyabinsk State University was supported by RSF-Russian Science Foundation project No. 17-72-20022 (computational studies). This work was supported by NSF Grants DMR-1904446 (M.E.J) and DMR-1905662 (D.H.). V.B. acknowledges support from the NUST "MISiS" No. K2-2020-018 B.B. acknowledges support from the COST Action CA16218.

- ¹P. C. Canfield, P. L. Gammel, and D. J. Bishop, *Physics Today* **51**, 40 (1998).
- ²P. A. Lee, N. Nagaosa, and X.-G. Wen, *Rev. Mod. Phys.* **78**, 17 (2006).
- ³Y. Mizuguchi and Y. Takano, *J. Phys. Soc. Japan* **79**, 102001 (2010).
- ⁴M. D. Lumsden and A. D. Christianson, *J. Phys: Conds. Mater.* **22**, 203203 (2010).
- ⁵Y. Du *et al.*, *EPL (Europhys. Lett.)* **103**, 37011 (2013).
- ⁶A. Bansil, S. Kaprzyk, P. Mijnaerends, and J. Tobiła, *Phys. Rev. B* **60**, 13396 (1999).
- ⁷L. R. Testardi, T. Wakiyama, and W. A. Royer, *J. Appl. Phys.* **48**, 2055 (1977).

- ⁸S. Ohshima, H. Ishida, T. Wakiyama, and K. Okuyama, *Japan Soc. Appl. Phys.* **28**, 1362 (1989).
- ⁹M. Jamer et al., *Phys. Rev. B* **91**, 094409 (2015).
- ¹⁰G. Gao and K. Yao, *Appl. Phys. Lett.* **103**, 232409 (2013).
- ¹¹I. Galanakis, S. Tirpanci, K. Özdoğan, and E. Şaşıoğlu, *Phys. Rev. B* **94**, 064401 (2016).
- ¹²W. Markiewicz et al., *IEEE Trans. Magnets.* **13**, 35 (1977).
- ¹³B. T. Matthias, E. A. Wood, E. Corenzwit, and V. B. Bala, *J. Phys. Chem. Solids* **1**, 188 (1956).
- ¹⁴M. Weger, *Rev. Mod. Phys.* **36**, 175 (1964).
- ¹⁵Y. A. Izyumov and Z. Kurmaev, *Sov. Phys. Uspekhi* **17**, 356 (1974).
- ¹⁶L. R. Testardi, *Rev. Mod. Phys.* **47**, 637 (1975).
- ¹⁷B. M. Klein, L. L. Boyer, D. A. Papaconstantopoulos, and L. F. Mattheiss, *Phys. Rev. B* **18**, 6411 (1978).
- ¹⁸T. Jarlborg and P. O. Nilsson, *J. Phys. C: Sol. State Phys.* **12**, 265 (1979).
- ¹⁹A. Jain et al., *APL Materials*, 011002 (2013).
- ²⁰M. Jamer et al., *Appl. Phys. Lett.* **109**, 182402 (2016).
- ²¹M. E. Jamer et al., *Phys. Rev. Appl.* **7**, 064036 (2017).
- ²²B. He et al., *Phys. Stat. Sol. (RRL)* **13**, 1900483 (2019).
- ²³A. A. Coelho, *J. Appl. Crystallogr.* **51**, 210 (2018).
- ²⁴S. Foner, E. McNiff Jr, S. Moehlecke, and A. Sweedler, *Sol. State Commun* **39**, 773 (1981).
- ²⁵D. Decker and H. Laquer, *J. Appl. Phys.* **40**, 2817 (1969).
- ²⁶G. Kresse and J. Furthmüller, *Phys. Rev. B* **54**, 11169 (1996).
- ²⁷G. Kresse and D. Joubert, *Phys. Rev. B* **59**, 1758 (1999).
- ²⁸J. P. Perdew and A. Zunger, *Phys. Rev. B* **23**, 5048 (1981).
- ²⁹J. Perdew, *Physica B: Conds. Mater.* **172**, 1 (1991).
- ³⁰K. Burke, J. Perdew, and M. Ernzerhof, *Int. J. Quant. Chem.* **61**, 287 (1997).
- ³¹J. Perdew, K. Burke, and M. Ernzerhof, *Phys. Rev. Lett.* **77**, 3865 (1996).
- ³²J. P. Perdew, S. Kurth, A. c. v. Zupan, and P. Blaha, *Phys. Rev. Lett.* **82**, 2544 (1999).
- ³³J. Tao, J. P. Perdew, V. N. Staroverov, and G. E. Scuseria, *Phys. Rev. Lett.* **91**, 146401 (2003).
- ³⁴J. Sun, A. Ruzsinszky, and J. P. Perdew, *Phys. Rev. Lett.* **115**, 036402 (2015).
- ³⁵M. Jamer et al., *Supplemental Information* (2020).
- ³⁶E. B. Isaacs and C. Wolverton, *Phys. Rev. Mater.* **2**, 063801 (2018).
- ³⁷Y. Fu and D. J. Singh, *Phys. Rev. Lett.* **121**, 207201 (2018).
- ³⁸M. Ekholm et al., *Phys. Rev. B* **98**, 094413 (2018).
- ³⁹D. Mejia-Rodriguez and S. B. Trickey, *Phys. Rev. B* **98**, 115161 (2018).
- ⁴⁰V. D. Buchelnikov et al., *Phys. Rev. B* **99**, 014426 (2019).

Supplementary Material for "Superconducting and Antiferromagnetic Properties of Dual-Phase V₃Ga"

Details and Results of the VASP calculations

The geometric optimization and ground state calculations were performed for two structures (D0₃ and A15) of V₃Ga, which are experimentally observed. In the case of D0₃ structure, the 16 atoms supercell was considered, in which Ga atoms locate at 4*a* (0.0, 0.0, 0.0) Wyckoff positions and V atoms take 4*b* (1/2, 1/2, 1/2) and 8*c* ((1/4, 1/4, 1/4) and 3/4, 3/4, 3/4) sites. For A15 structure, six-atom supercell was assumed, in which two Ga atoms occupy 2*a* sites and six V atoms locate at 6*c* sites. Concerning to magnetic subsystem, ferromagnetic (FM) and antiferromagnetic (AFM) spin alignments of V atoms were considered. For D0₃ structure, FM and AFM G-type orders were considered according to Ref. [11], while for A15 structure, FM and three AFM orders were proposed in accordance with Ref. [22]. The crystal structures as well as the magnetic configuration considered are illustrated in Fig. 1. To emphasize the AFM order, V atoms located at different sites were distinguished by labels 1, 2, and 3.

To consider the exchange-correlation effects, the following functionals were assumed in the electronic calculations: LDA-PZ [28], GGA-PBE [29–31], GGA+*U* and meta-GGA-SCAN [32–34] parametrizations. For GGA+*U* scheme, the values of Hubbard-repulsion *U* and Hund-exchange integral *J* for V atoms were taken 2 and 0.67 eV, correspondingly, in accordance with He *et al.* [22]. The PAW pseudopotentials were taken with valence-electron configurations as follows: 3*s*²3*p*⁶4*s*²3*d*³ for V atoms and 3*d*¹⁰4*s*²4*p*¹ for Ga atoms. The 10×10×10 *k*-points grid was generated using Monkhorst-Pack scheme. The kinetic-energy cutoff for the augmented charge was taken 750 eV. The Methfessel-Paxton smearing method [?] was used with a width of 0.2 eV in geometry optimization runs, and the tetrahedron smearing method with Blóchl corrections [?] was deployed in self-consistent calculations. The calculations were converged to an accuracy of 10⁻⁸ eV. The convergence criterion in the optimization for the residual forces was 10⁻⁷ eV/Å.

The results of *ab initio* calculations for D0₃ and A15 crystal structures of V₃Ga are presented in Tables 1 and 2, respectively.

Details and Results of the SPR-KKR calculations

The calculations of the Heisenberg's exchange coupling parameters (J_{ij})

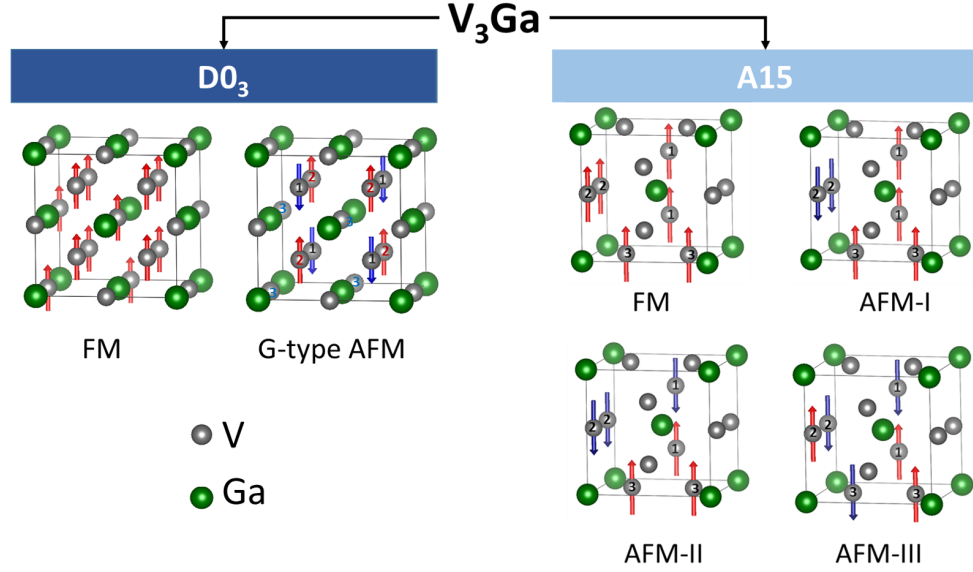


Figure 1: Types of the magnetic ordering for $D0_3$ and $A15$ structures used in calculations for V_3Ga . V atoms located at different sites are noted by labels 1, 2, and 3.

Table 1: The equilibrium lattice parameter (a_0 in Å), partial and total magnetic moments (μ_{V_i} and μ_{tot} in μ_B /f.u.), and total energy (E in eV/atom) of non-magnetic (NM) and AFM phases of $D0_3$ structure. Notice, the initial FM order was converged to the non-magnetic (NM) one.

NM						
	a_0	μ_{V_1}	μ_{V_2}	μ_{V_3}	μ_{tot}	E
LDA	5.899	0.00	0.00	0.00	0.00	-8.486
PBE	6.034	0.00	0.00	0.00	0.00	-7.574
PBE+ U	6.059	0.00	0.00	0.00	0.00	-6.541
SCAN	5.977	0.00	0.00	0.00	0.00	-17.377
AFM						
	a_0	μ_{V_1}	μ_{V_2}	μ_{V_3}	μ_{tot}	E
LDA	5.902	-0.429	0.429	0.00	0.00	-8.487
PBE	6.064	-1.314	1.314	0.00	0.00	-7.600
PBE+ U	6.130	-1.916	1.916	0.00	0.00	-6.647
SCAN	6.035	-1.848	0.00	1.848	0.00	-17.486

were performed using of the spin-polarized scalar-relativistic (SP-SREL) Dirac-Hamiltonian as part of the SPR-KKR (A spin-polarized relativistic Korringa-

Table 2: The equilibrium lattice parameter (a_0 in Å), partial and total magnetic moments (μ_{V_i} and μ_{tot} in μ_B /f.u.), and total energy (E in eV/atom) of FM and AFM phases of A15 structure.

FM						
	a_0	μ_{V_1}	μ_{V_2}	μ_{V_3}	μ_{tot}	E
LDA	4.678	0.089	0.164	0.112	0.368	-8.572
PBE	4.788	0.222	0.390	0.303	0.916	-7.645
PBE+ U	4.817	0.434	0.661	0.548	1.636	-6.601
SCAN	4.744	0.308	0.523	0.414	1.244	-17.442
AFM-I						
	a_0	μ_{V_1}	μ_{V_2}	μ_{V_3}	μ_{tot}	E
LDA	4.678	0.097	0.122	0.147	0.368	-8.572
PBE	4.788	0.248	0.306	0.361	0.916	-7.645
PBE+ U	4.828	0.576	0.307	0.760	1.636	-6.602
SCAN	4.742	0.00	0.00	0.00	0.00	-17.436
AFM-II						
	a_0	μ_{V_1}	μ_{V_2}	μ_{V_3}	μ_{tot}	E
LDA	4.677	0.00	0.00	0.00	0.00	-8.572
PBE	4.786	0.00	0.00	0.00	0.00	-7.643
PBE+ U	4.801	± 1.036	± 0.024	± 0.007	0.00	-6.594
SCAN	4.742	± 0.355	± 0.002	± 0.017	0.00	-17.436
AFM-III						
	a_0	μ_{V_1}	μ_{V_2}	μ_{V_3}	μ_{tot}	E
LDA	4.678	0.00	0.00	0.00	0.00	-8.572
PBE	4.788	0.00	0.00	0.00	0.00	-7.643
PBE+ U	4.879	± 1.351	± 1.508	± 1.502	0.00	-6.632
SCAN	4.744	± 0.268	± 0.326	± 0.330	0.00	-17.437

Kohn-Rostoker) package [?]. For these calculations, the optimized lattice parameter obtained by VASP calculation for FM phase of D0₃ structure has been used. It should be noted that in this case, calculations were carried out for unit cell of D0₃ consisting of four atoms (3 V and 1 Ga). The exchange-correlation energy was treated by the GGA-PBE parameterization [30]. For the self-consistent cycles calculations, 2300 k -points were generated by a k -mesh grid of 45³. The angular momentum expansion (l_{max}) was restricted to three. The magnetic exchange constants were calculated on a k -mesh grid of 57 × 57 × 57 with 4495 k -points. All calculations converged to 0.01 mRy of total energy. The dependence of the exchange interaction parameter J_{ij} on the distance between atoms d/a is shown in Fig. 2.

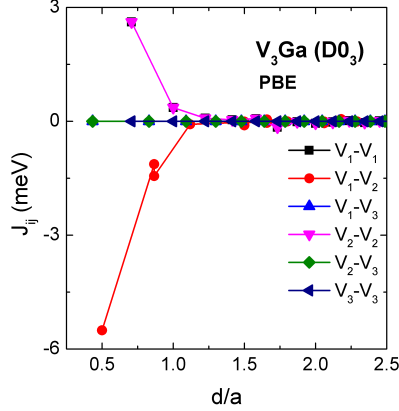


Figure 2: Exchange coupling constants J_{ij} as a function of distance (d/a) between atoms i and j for V_3Ga with $D0_3$ structure at their equilibrium lattice parameter

Here, the positive exchange constants ($J_{ij} > 0$) presented FM coupling, whereas the negative ones ($J_{ij} < 0$) indicate AFM coupling. It is obvious that the large FM interactions are observed between nearest neighbors V_1 - V_1 and V_2 - V_2 atoms. The magnitudes of these couplings are the same and about of 3 meV. While, they reduces sufficiently and becomes zero in the third and further coordination shells. The strongest AFM interaction (-5.5 meV) is observed between the nearest V_1 and V_2 atoms located at different sublattices. The all interactions with V_3 atoms are close to 0 meV during the zero magnetic moment in V_3 atoms (See, Table 1).

Details and Results of the Monte Carlo simulations

To extend the zero-temperature *ab initio* results to finite temperatures, we further performed the Monte Carlo (MC) simulations of the classical three-dimensional Heisenberg model ($\mathcal{H} = \sum_{ij} J_{ij} S_i S_j$) in zero magnetic field. Here, $\mathbf{S}_i = (S_i^x, S_i^y, S_i^z)$ is a classical Heisenberg spin variable $|S_i| = 1$ and J_{ij} are the exchange coupling constants (positive in case of FM interactions and negative in case of AFM interactions depending on the distance between the atoms). The calculated exchange parameters (J_{ij}) and partial magnetic moments (μ_i) were taken as input parameters. Since, the J_{ij} behavior versus the distance between atoms (d/a) shows the long-range oscillation trend, therefore we restricted exchange interactions up to sixth coordination shell for all interaction pairs.

The MC simulations were carried out for a simulation lattice with real unit cell consisting of 3925 atoms (1099 Ga and 2826 V atoms) and periodic

boundary conditions by using the Metropolis algorithm [?], where, some new, random spin direction is chosen and the energy change which would result if this new spin orientation is kept, is then calculated. Changes of the independent spin variables $\mathbf{S}_i = (S_i^x, S_i^y, S_i^z)$ are accepted or rejected according to the single-site transition probability $W = \min[1, \exp(-\Delta\mathcal{H}/k_B T)]$. As a time unit, we used one MC step consisting of N attempts to change the spin variables. A new spin direction can be chosen by randomly choosing new spin components. The spin components are chosen in the following manner [?]. Two random numbers r_1 and r_2 are chosen from the interval $[0, 1]$ to produce a vector with two components $\zeta_1 = 1 - 2r_1$ and $\zeta_2 = 1 - 2r_2$. The length of the vector is determined by $\zeta^2 = \zeta_1^2 + \zeta_2^2$ and if $\zeta^2 < 1$, then a new spin vector is computed with components

$$S_i^x = 2\zeta_1\sqrt{1 - \zeta^2}, \quad S_i^y = 2\zeta_2\sqrt{1 - \zeta^2}, \quad S_i^z = 1 - 2\zeta^2.$$

For each temperature the properties (internal energy of the system $\langle \mathcal{H} \rangle$ and magnetic order parameter $\langle m \rangle$) were estimated allowing 10^5 MC steps and 10^4 thermalization steps and were averaged over 2250 configurations for each 400 MC steps. The simulation started from the ferromagnetic phase with $S_i^z = 1$.

The magnetic order parameter is defined by the following way

$$m^\alpha = \frac{1}{N^\alpha} \sum_i \sqrt{(S_i^{\alpha,x})^2 + (S_i^{\alpha,y})^2 + (S_i^{\alpha,z})^2},$$

where α denotes V_1 , V_2 and V_3 atoms and N^α the total number of α atoms; i runs over the corresponding lattice sites of the α atoms. The resulting temperature dependencies of partial magnetizations of $V_{1,2}$ for $V_3\text{Ga}$ with D0_3 alloy at zero magnetic field is shown in Fig. 3.

In order to estimate the Neél temperature, we plotted $m(T) = (m^\alpha)^{1/\beta}(T)$ function, which approximately linear decreases with increasing temperature. The Neél temperature can be estimated at the intersection of m with the T axis. Here, m^α is the partial magnetization of V_1 , V_2 atoms and β is the critical index. Note, in the case of the three-dimensional Heisenberg model the β exponent is equal to 0.3646. Estimation give us Neél temperature $T_N = 587$ K.

Results of Disorder Calculations

The effects of disorder on the Neél transition temperature was computed with SPR-KKR package and KKR-CPA approach. The degree of disorder in the atomic sublattices was quantified by x , given by the fraction of Ga

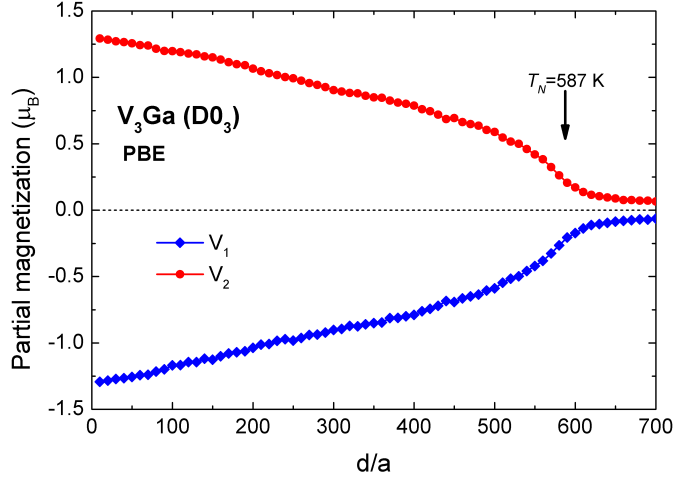


Figure 3: Temperature variation of the partial magnetization curves for V_3Ga compound with $D0_3$ structure at zero magnetic field.

Table 3: Partial magnetic moments of V_i atoms, as well as Néel temperatures calculated for $D0_3$ phase of V_3Ga with different degree of disorder. Note, that a disorder with degree 0 means ordered $D0_3$ phase.

Degree of disorder	μ_{V_1}	μ_{V_2}	μ_{V_3}	μ_{V_4}	μ_{tot}	T_N
0	-1.161	1.161	0.00	-	0.00	630.0
0.05	-0.997	0.997	0.00	0.00	0.00	414.5
0.1	-0.720	0.720	0.00	0.00	0.00	189.3
0.2	0.002	0.002	0.00	0.00	0.00	0.00

atoms that are exchanged for nonmagnetic V atoms (labeled V_3), where the nonmagnetic V atoms lie between the two antiferromagnetically coupled magnet V atoms (labeled V_1 and V_2). The results of the calculations are shown in Table 3 for $x = 0$ to 0.2. For all those values of x , the V_1 and V_2 magnetic atoms have opposite signs and equal magnitudes, while the V_3 moment is zero. The Néel temperature is seen to decrease from $T_N = 630$ K at $x = 0$ to $T_N = 0$ at $x = 0.2$. Figure 5 in the main text shows T_N as a function of x .

Results of Rietveld X-ray Diffraction Analysis

X-ray diffraction of the V_3Ga sample was taken at Beamline 11-BM at the Advanced Photon Source at Argonne National Lab using a wavelength of $\lambda = 0.413841 \text{ \AA}$ and the sample was rotated continuously. Figure 4 shows the XRD data and subsequent Rietveld and Pawley fitting procedures. [23] The experimental data is shown by the points and fit to the data is shown by the pink curve. The lower blue curve plots the experimental data minus the Rietveld fit. In this figure, only the A15, $D0_3$ and A2 phases were included as part of the Rietveld fitting procedure. The A2 phase is a disordered $D0_3$ phase where the V and Ga are randomly exchanged. Only including those three phases, it was determined that another phase was present. A search of relevant V, Ga and V-Ga binary phases (V_6Ga_5 , V_6Ga_7 , V_2Ga_5) were unable to accurately index the remaining peaks. Thus, an expanded search to contain impurity oxide phases was done. Through this, it was determined that the remaining peaks could be accurately indexed to a reported oxide impurity phase, V_3GaO_x . [?] The structure of the V_3GaO_x phase is not rigorously reported; however, the previous work discussed the structure as Cu_3Au -type perovskite with Ga at the corners, V at the face centers and O at the body center. From this, a structure was built and space group determined through the use of Python Materials Genomics library. [?] Since the structure of the V_3GaO_x has not been determined as well as its existence as a minor impurity phase in the current work, its contribution to the X-ray diffraction pattern was modeled only by a Pawley refinement procedure. As such, the weight fraction of the V_3GaO_x phase cannot be determined and all other reported weight fractions for the A15, $D0_3$, and A2 phases are reported relative to each other. The results of the fitting procedure provided the following approximate percentages of the various phases: 81% in the A15 phase, 18% in the $D0_3$ phase, and 0.1% in the A2 phase. An attempt to include the determined structure for the V_3GaO_x phase for Rietveld refinement yielded an approximate weight fraction on the order of 30 - 40%.

Analysis of superconductivity of A15 phase

Additional analysis of the as-synthesized superconducting properties of the A15 V_3Ga revealed superconducting critical temperature of 13.6 K and a superconducting volume fraction at 2 K of approximately 90% as shown in Fig 5. This was calculated from the density and phase fraction extracted

from Rietveld analysis from synchrotron X-ray diffraction data for the A15 phase. Isothermal magnetization at 10 K revealed an upper critical field,

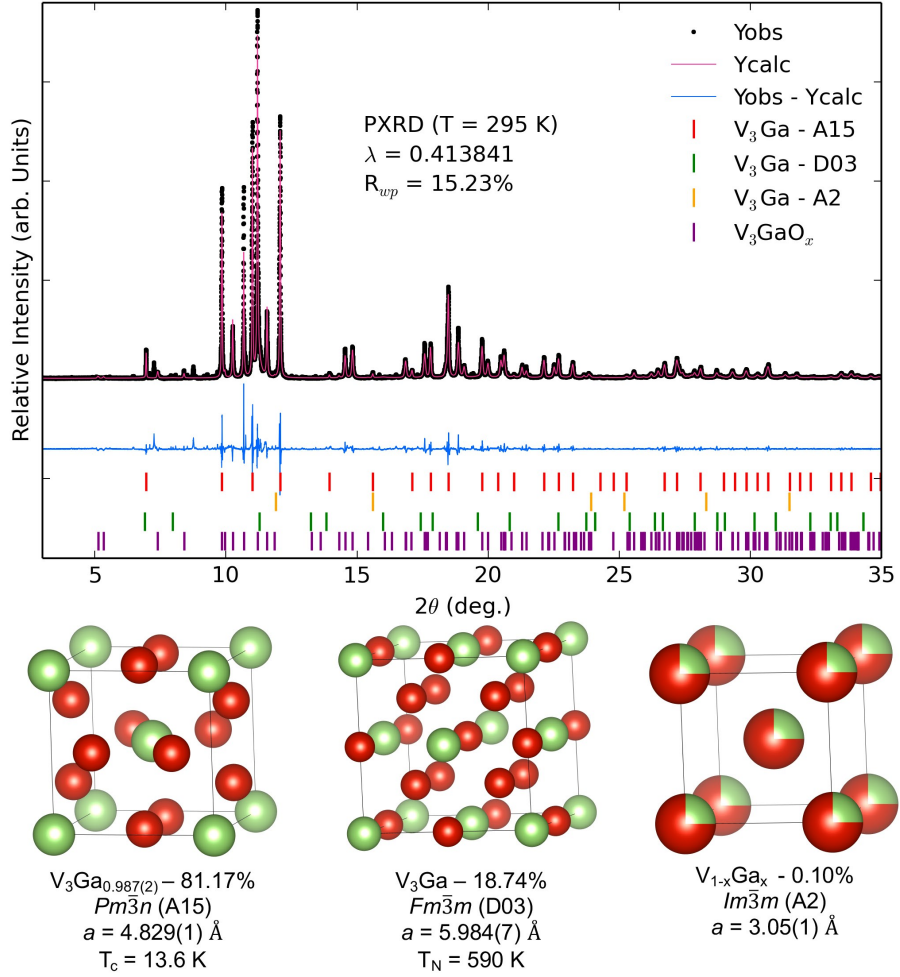


Figure 4: High resolution synchrotron X-ray diffraction patterns for as-grown V₃Ga ingots collected at T = 295 K. Red tick and green tick marks represent the targeted V₃Ga phases, A15 and D0₃ phases respectively. Orange tick marks represent impurity A2 phase and purple tick marks shown the existence of an impurity oxide phase, V₃GaO_x. These are shown below the calculated, observed, and differences curves from Rietveld analysis. Crystal structures, corresponding extracted lattice parameters and elemental composition from Rietveld analysis, and relevant transition temperature for each phase are shown below the XRD data.

H_{c2} of about 3.5 T which is significantly lower than previous reports. [24,25] This may be due to a number of factors such as stoichiometric changes in the as-synthesized A15 V_3Ga phase as well as the coexistence of another magnetic phase due to the V_3Ga $D0_3$ phase in the as-synthesized sample. Thus, the assignment of an H_{c2} value to the A15 V_3Ga phase cannot be done in a rigorous way. However, the extracted superconducting volume fraction and superconducting critical temperature matches with expectations.

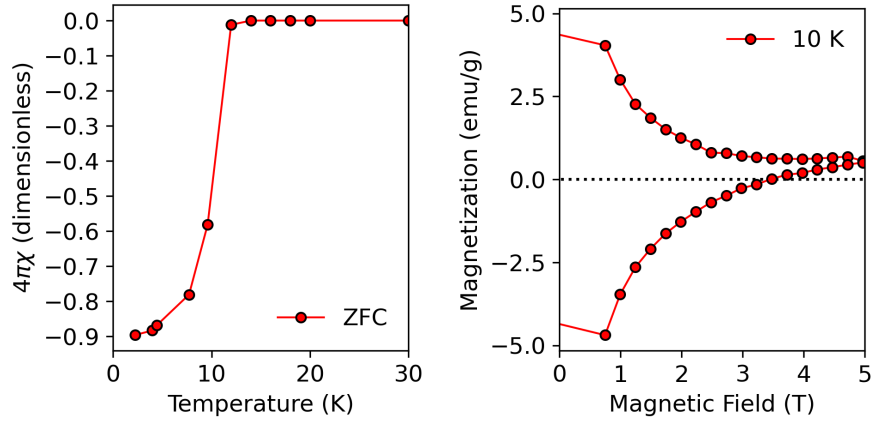


Figure 5: Temperature dependence of dimensionless magnetic susceptibility at 500 Oe and isothermal magnetization at 10 K of V_3Ga sample mixture measured on as-synthesized polycrystalline material.

References

- [1] P. C. Canfield, P. L. Gammel, and D. J. Bishop, *Physics Today* **51**, 40 (1998).
- [2] P. A. Lee, N. Nagaosa, and X.-G. Wen, *Rev. Mod. Phys.* **78**, 17 (2006).
- [3] Y. Mizuguchi and Y. Takano, *J. Phys. Soc. Japan* **79**, 102001 (2010).
- [4] M. D. Lumsden and A. D. Christianson, *J. Phys: Conds. Mater.* **22**, 203203 (2010).
- [5] Y. Du et al., *EPL (Europhys. Lett.)* **103**, 37011 (2013).
- [6] A. Bansil, S. Kaprzyk, P. Mijnaerends, and J. Toboła, *Phys. Rev. B* **60**, 13396 (1999).
- [7] L. R. Testardi, T. Wakiyama, and W. A. Royer, *J. Appl. Phys.* **48**, 2055 (1977).
- [8] S. Ohshima, H. Ishida, T. Wakiyama, and K. Okuyama, *Japan Soc. Appl. Phys.* **28**, 1362 (1989).
- [9] M. Jamer et al., *Phys. Rev. B* **91**, 094409 (2015).
- [10] G. Gao and K. Yao, *Appl. Phys. Lett.* **103**, 232409 (2013).
- [11] I. Galanakis, S. Tirpanci, K. Özdoğan, and E. Şaşıoğlu, *Phys. Rev. B* **94**, 064401 (2016).
- [12] W. Markiewicz et al., *IEEE Trans. Magnts.* **13**, 35 (1977).
- [13] B. T. Matthias, E. A. Wood, E. Corenzwit, and V. B. Bala, *J. Phys. Chem. Solids* **1**, 188 (1956).
- [14] M. Weger, *Rev. Mod. Phys.* **36**, 175 (1964).
- [15] Y. A. Izyumov and Z. Kurmaev, *Sov. Phys. Uspekhi* **17**, 356 (1974).
- [16] L. R. Testardi, *Rev. Mod. Phys.* **47**, 637 (1975).
- [17] B. M. Klein, L. L. Boyer, D. A. Papaconstantopoulos, and L. F. Mattheiss, *Phys. Rev. B* **18**, 6411 (1978).
- [18] T. Jarlborg and P. O. Nilsson, *J. Phys. C: Sol. State Phys.* **12**, 265 (1979).

- [19] A. Jain et al., *APL Materials* , 011002 (2013).
- [20] M. Jamer et al., *Appl. Phys. Lett.* **109**, 182402 (2016).
- [21] M. E. Jamer et al., *Phys. Rev. Appl.* **7**, 064036 (2017).
- [22] B. He et al., *Phys. Stat. Sol. (RRL)* **13**, 1900483 (2019).
- [23] A. A. Coelho, *J. Appl. Crystallogr.* **51**, 210 (2018).
- [24] S. Foner, E. McNiff Jr, S. Moehlecke, and A. Sweedler, *Sol. State Commun* **39**, 773 (1981).
- [25] D. Decker and H. Laquer, *J. Appl. Phys.* **40**, 2817 (1969).
- [26] G. Kresse and J. Furthmüller, *Phys. Rev. B* **54**, 11169 (1996).
- [27] G. Kresse and D. Joubert, *Phys. Rev. B* **59**, 1758 (1999).
- [28] J. P. Perdew and A. Zunger, *Phys. Rev. B* **23**, 5048 (1981).
- [29] J. Perdew, *Physica B: Conds. Mater.* **172**, 1 (1991).
- [30] K. Burke, J. Perdew, and M. Ernzerhof, *Int. J. Quant. Chem.* **61**, 287 (1997).
- [31] J. Perdew, K. Burke, and M. Ernzerhof, *Phys. Rev. Lett.* **77**, 3865 (1996).
- [32] J. P. Perdew, S. Kurth, A. c. v. Zupan, and P. Blaha, *Phys. Rev. Lett.* **82**, 2544 (1999).
- [33] J. Tao, J. P. Perdew, V. N. Staroverov, and G. E. Scuseria, *Phys. Rev. Lett.* **91**, 146401 (2003).
- [34] J. Sun, A. Ruzsinszky, and J. P. Perdew, *Phys. Rev. Lett.* **115**, 036402 (2015).
- [35] M. Jamer et al., *Supplemental Information* (2020).
- [36] E. B. Isaacs and C. Wolverton, *Phys. Rev. Mater.* **2**, 063801 (2018).
- [37] Y. Fu and D. J. Singh, *Phys. Rev. Lett.* **121**, 207201 (2018).
- [38] M. Ekholm et al., *Phys. Rev. B* **98**, 094413 (2018).
- [39] D. Mejia-Rodriguez and S. B. Trickey, *Phys. Rev. B* **98**, 115161 (2018).
- [40] V. D. Buchelnikov et al., *Phys. Rev. B* **99**, 014426 (2019).